Remote Sens. **2013**, *5*, 4470-4487; doi:10.3390/rs5094470

OPEN ACCESS

Remote Sensing

ISSN 2072-4292

www.mdpi.com/journal/remotesensing

Article

Extraction of Coastline in Aquaculture Coast from Multispectral Remote Sensing Images: Object-Based Region Growing Integrating Edge Detection

Tao Zhang [1,2], Xiaomei Yang [1,*], Shanshan Hu [3] and Fenzhen Su [1]

[1] State Key Laboratory of Resources and Environmental Information System, IGSNRR, CAS, Beijing 100101, China; E-Mails: zhangt@lreis.ac.cn (T.Z.); sufz@lreis.ac.cn (F.S.)

[2] University of Chinese Academy of Sciences, Beijing 100049, China

[3] College of Resource Environment and Tourism, Capital Normal University, Beijing 100048, China; E-Mail: hushshan@126.com

* Author to whom correspondence should be addressed; E-Mail: yangxm@lreis.ac.cn; Tel.: +86-10-6488-8955; Fax: +86-10-6488-9630.

Received: 20 May 2013; in revised form: 29 August 2013 / Accepted: 3 September 2013 / Published: 12 September 2013

Abstract: Aquaculture coasts have become widely distributed in coastal zones as human activities are intensified. Due to the complexity in this type of coast, it is difficult to extract the coastline with traditional automated mapping approaches. In this paper, we present an automated method—*object-based region growing integrating edge detection* (OBRGIE) for the extraction of this type of coastline. In this method, a new object feature named *OMI* (*object merging index*) is proposed to separate land and sea. The OBRGIE method was applied to Landsat Thematic Mapper (TM) (pixel size 30m) and Satellite Pour l'Observation de la Terre (SPOT-5) (pixel size 10 m) images of two coastal segments with lengths of 272.7 km and 35.5 km respectively, and the accuracy of the extracted coastlines was assessed in comparison with the manually delineated coastlines. The mean and RMSE (root mean square error) are 16.0 m and 16.4 m respectively for the TM images, and 8.0 m and 8.6 m, respectively, for the SPOT-5 images, indicating that the proposed method derives coastlines with pixel accuracy. The OBRGIE method is also found to be robust to the segmentation scale parameter, and the *OMI* feature is much more effective than the spectral attribute in separating land and sea in aquaculture coasts. This method may provide an inexpensive means of fast coastline mapping from remotely sensed imagery with relatively fine-to-moderate spatial resolution in coastal sectors with intense human interference.

Keywords: coastline extraction; aquaculture; image segmentation; region growing; edge detection; object merging index

1. Introduction

Coastline is the boundary of the land and ocean masses, and knowledge of the coastline is the basis for measuring and characterizing the resources and environment of the land and ocean. Automated analyses of the coastline, or coastline mapping techniques, have been pursued [1,2]. In practice, different types of seacoasts, such as bedrock, artificial, arenaceous, silty, and biological coasts, have their own characteristics, which impose different degrees of complexity on coastline mapping [3].

As a special type of complex artificial coast, aquaculture coast is formed by the farming of aquatic organisms on silt tidal flats. With the rapid growth of coastal aquaculture in recent years, aquaculture coasts have increased in some developing countries. It has been estimated that aquaculture coasts constitute about 30% of all coastlines in mainland China [4]. In order to identify, monitor, model, and manage the vast expanse of coastal aquaculture, effective methods of extracting aquaculture coastlines from remotely sensed imagery are desired.

Automated methods of extracting coastlines from remote sensing imagery can be generally grouped into four categories: (1) the edge detection approaches, which treat the extraction of coastline as an edge detection problem [5]; (2) the band thresholding methods, in which a thresholding value is selected either by man-machine interaction or by a local adaptive strategy [6,7]. As this method is easy to implement and can obtain good accuracy for most coast types, it is widely used in coastline detection applications [8–10]; (3) the classification approaches, which aim to separate the image into land and water components, and then take the boundary line between them as the coastline. The supervised classification [11], unsupervised classification [12], soft classification [13,14], and association rule method [3] belong to this category; 4) the fusion techniques [2], which combine two or more data sources including optical, SAR (Synthetic Aperture Radar), and LIDAR (LIght Detection And Ranging) data for coastline extraction [15,16].

However, applying these methods to delineating aquaculture coasts may not be successful as these coasts have two special characteristics (Figure 1a): (*i*) both the aquaculture region and the ocean area are covered by water body with similar spectral attributes; (*ii*) the aquaculture zone and ocean are always spatially adjacent or even connected by narrow channels. Therefore, it would be difficult for the band thresholding and classification approaches to separate the aquacultural pond water from ocean water based on spectral attributes. The edge detection approaches may also encounter difficulties because so many edges exist in aquacultural regions (Figure 1b) that it is hard to identify and link the right edges for coastlines.

By analyzing remotely sensed images of aquaculture coasts, we note that the common boundaries between the ocean and aquaculture ponds are quite clear in most cases, though the width of these boundaries is quite narrow, only one to two pixels in TM images. Moreover, the edge information is likely to play an important role in separating the sea from the aquacultural region, considering the

failure of spectral features, as long as the edge features between the ocean and the aquacultural region can be identified and distinguished from those inside the aquaculture region.

Figure 1. Illustration of spectral and spatial complexities of aquaculture coasts. (**a**) SPOT5 grey image of near-infrared band; (**b**) edge information extraction by the Canny algorithm.

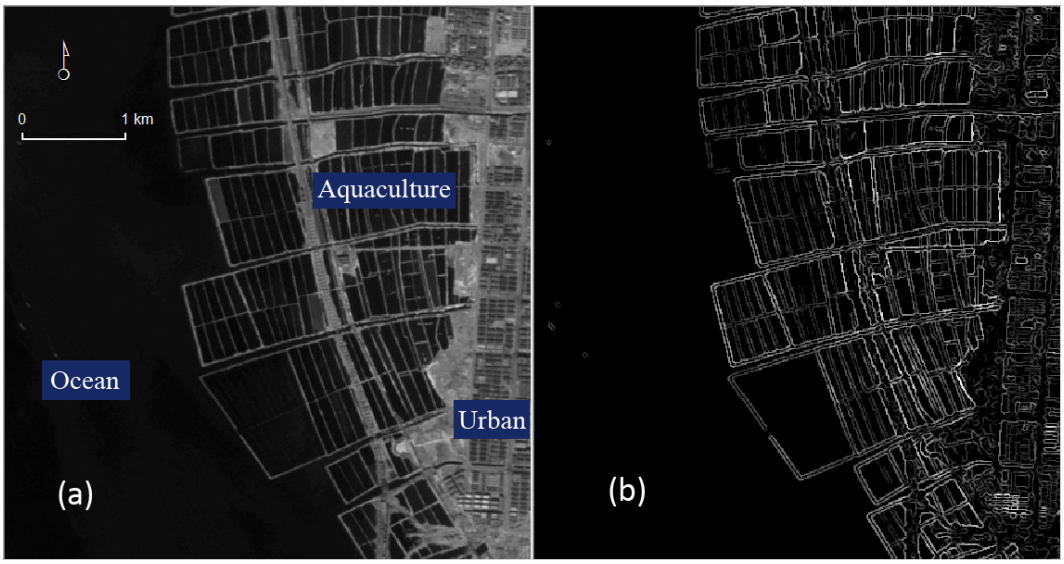

In this study, we present a method, integrating image segmentation, region growing, and edge detection, to delineate aquaculture coastlines. This integrated procedure is called *object-based region growing integrated with edge detection* (OBRGIE), and a new feature *object merging index* (*OMI*) is proposed to integrate edge information into the processing of region growing. The influence of segmentation scale parameter on the OBRGIE method is assessed and the effectiveness of *OMI* is evaluated as well.

2. Case Background—Location and Data

Before getting into details of the method, background information of the cases to be studied is introduced. To evaluate the applicability of the methods in different locations, two sites were selected for case studies (Figure 2). One site is located in the Bohai Sea in Northern China, with a coastline sector of 272.7 km and abundant aquaculture ponds and salt pans along the coastline. In addition, a large area of land has been reclaimed from the sea for urban construction in the lower central part of the area. The other site is located in the Zhujiangkou Estuary in Southern China, with a coastline sector of 35.5 km. This coastal area has been greatly urbanized, and large area of aquaculture ponds is distributed along the north part of the coast.

Two different data sources are used in this study. A Landsat Thematic Mapper (TM) image, acquired on 30 August 2009, is used for the Bohai case, which consists of six multispectral bands. For the Zhujiangkou case, a SPOT-5 multispectral image, acquired on 9 November 2010, is used, which consists of four multispectral bands. The main parameters for the Landsat TM and SPOT-5 images are shown in Table 1.

Figure 2. Study area and images used in this study. (**a**) TM image for the Bohai case; (**b**) SPOT-5 image for the Zhujiangkou case. The yellow lines indicate the "true" coastline obtained by manual interpretation.

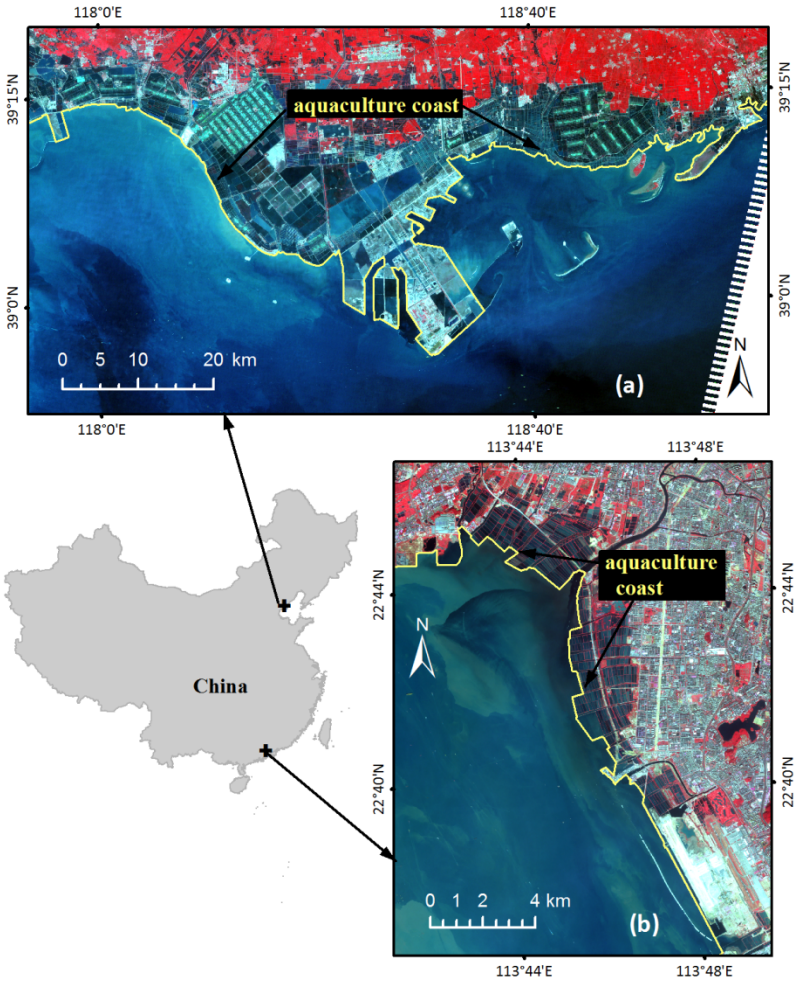

Table 1. Band wave length and pixel size for Landsat Thematic Mapper (TM) and SPOT-5 images.

Landsat TM			SPOT-5		
Band No.	**Wavelength (nm)**	**Pixel Size**	**Band No.**	**Wavelength (nm)**	**Pixel Size**
1	0.45–0.52	30 m	1	0.50–0.59	10 m
2	0.52–0.60	30 m	2	0.61–0.68	10 m
3	0.63–0.69	30 m	3	0.78–0.89	10 m
4	0.76–0.90	30 m	4	1.58–1.75	20 m
5	1.55–1.75	30 m			
7	2.08–2.35	30 m			

In order to assess the accuracy of the coastline extracted by the automated approaches, the "true" coastlines are prepared in advance by the method of visual interpretation. The image source used in manual interpretation for the Bohai case is pansharpened SPOT-5 multispectral imagery (2.5 m per pixel), aquired in 2008, and TM image is used where coastline has changed from 2008 to 2009. For the Zhujiangkou case, the true coastline is delineated manually from the pansharpened SPOT-5 image (2.5 m per pixel) acquired in 2010. The manually delineated "true" coastline is shown in yellow in

Figure 2a,b. Four coastline transacts were obtained by field survey with differential GPS in 2010 for the Bohai case, and comparison between the field survey line segments and the manually delineated coastline shows an average difference of 2.1 m, indicating good positioning accuracy of the manually interpreted coastlines.

3. Methodology

The coastline extraction method of OBRGIE is first presented in this section, and then the method of accuracy assessment is introduced. Multi-scale analysis is performed in order to test the robustness of the OBRGIE method on the segmentation scale parameter. The method of region growing with spectral attributes (RGSA) is also introduced for coastline extraction in comparison with the OBRGIE method.

Figure 3. Flow chart of the OBRGIE method for coastline extraction.

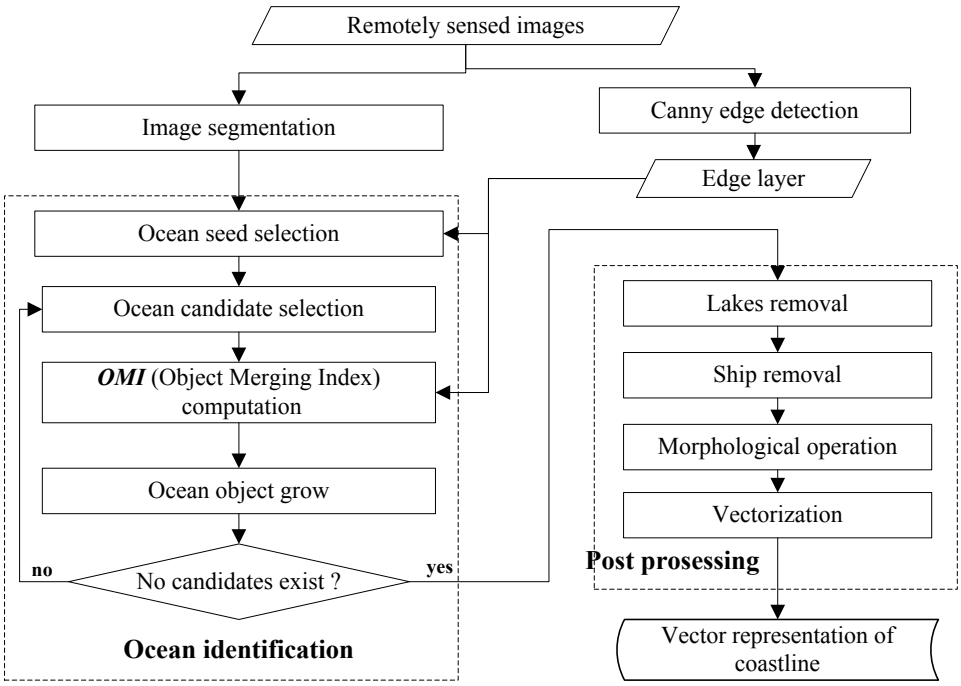

3.1. The OBRGIE Method for Coastline Extraction

The OBRGIE method includes four main processes, as shown in the flowchart in Figure 3, and separating the sea and aquaculture region is essential. The first step performs image segmentation and prepares the object primitives. The second step implements edge detection and provides edge information. The third step is the most essential, which identifies the ocean seeds and candidates, and lets the ocean area grow to, and only to, the land-ocean boundary. The final step performs post-processing, in which unnecessary objects are removed and the coastline is refined. Details of the procedures are described in the following sections through step-by-step processing of a subset of SPOT-5 images, illustrated in Figure 4.

3.1.1. Image Segmentation

Segmentation is conducted using the multiresolution segmentation algorithm [17] provided in eCognition™ [18]. This algorithm has been used in many applications [19–23]. An image is partitioned into object primitives, which have small internal spectral heterogeneity with respect to their neighboring objects. This algorithm requires three user-defined parameters to control the size and shape of the generated image objects: (*1*) scale, (*2*) shape weight, and (*3*) compactness weight. The shape weight is fixed to be 0.5 and the compactness weight is fixed to be 0.2 for the images processed in this study as experiments show that this parameter setting can achieve good object shape for aquaculture ponds. The scale value controls the extent of the image object primitives, and may affect the accuracy of extracted coastline. The effect of the segmentation scale parameter on the coastline extraction is discussed in Section 3.3. An example of segmented image can be found in Figure 4c with scale setting of 15.

Figure 4. Illustration of coastline extraction by the OBRGIE method: (**a**) image subset of SPOT-5 NIR band; (**b**) edge layer by the Canny detector; (**c**) image segments; (**d**) 'obj 1' is selected as seed, but 'obj 2' is not; (**e**) seed selection (blue); (**f**) candidate selection (green); (**g**) ocean object growing result; (**h**) coastline after morphological operation; and (**i**) vectorized coastline (red).

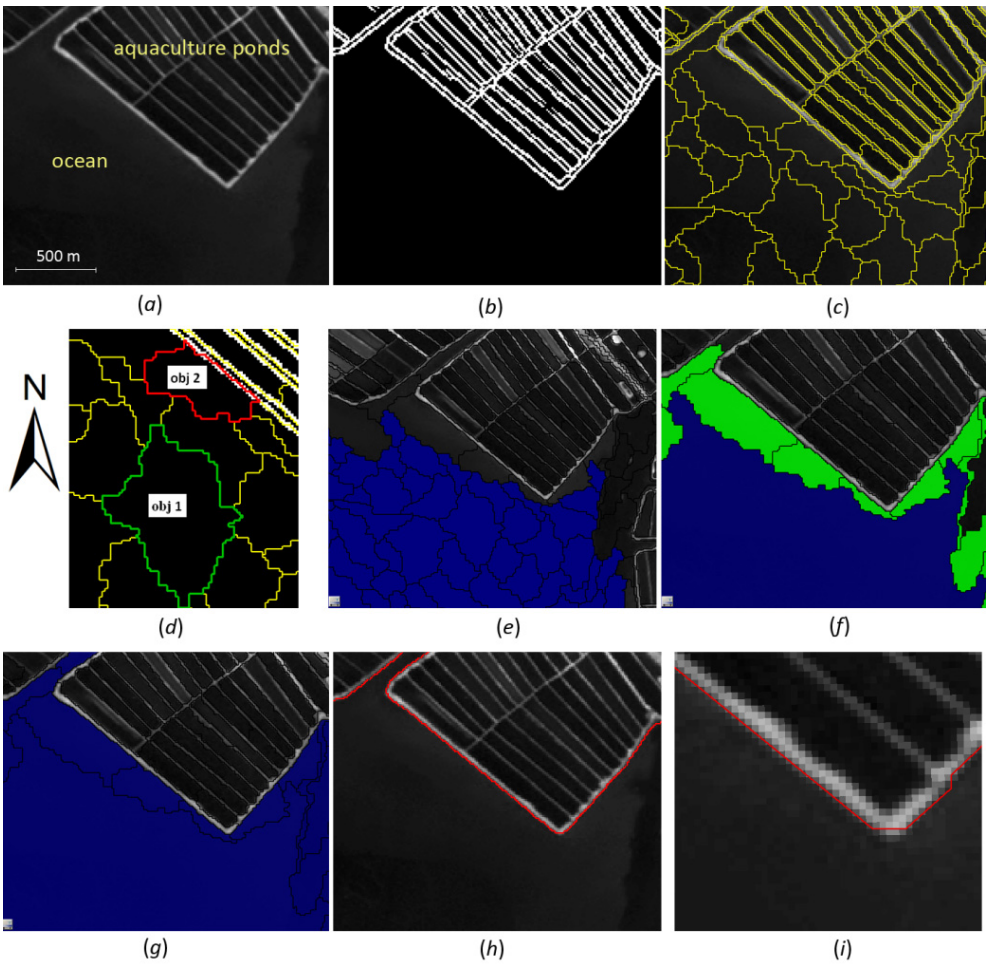

3.1.2. Edge Layer Generation

The Canny edge detection algorithm [24] is employed to identify the edge pixels in the image, and the edge detector is applied to the near-infrared (NIR) bands (band-3 for SPOT-5 and band-5 for TM) as the edges of land and water are sharp in these bands. This edge detection step produces an edge intensity layer, in which the pixels with intensity value greater than zero are considered to be "edge pixels". Edge detection for the subimage is shown in Figure 4b, in which white pixels represent edge pixels and black pixels represent non-edge background.

3.1.3. Ocean Identification by Region Growing

The following procedures are used for ocean identification:

(1) identify ocean seed objects;
(2) identify candidate objects;
(3) grow ocean seeds to proper candidates;
(4) repeat step (2) and step (3) until no candidates can be merged.

Ocean Seed Objects Identification

Ocean seed is selected in an automated way in this step. In order to select the water objects from the ocean region as ocean seeds, and filter out the water objects from the aquaculture region, the seed objects should meet two requirements: (1) they should be edge free because the center area of the ocean region seldom contains edge pixels; (2) they should be a water body. The second requirement can be realized by evaluating the NIR band intensity, which is sensitive to water and non-water substance, and the NIR bands used in this study are band-3 for SPOT-5 and band-5 for TM imagery.

For the first requirement, we propose a new object feature—*seed_index*, which is calculated as follows: (*i*) segment the selected object into pixels by chessboard segmentation [18] and create an object level below (pixel level); (*ii*) identify the border pixels for the object (see Figure 5a), and count the number of border pixels as N_b; (*iii*) identify the edge pixels (edge layer value > 0) among the border pixels, and count the number of edge pixels as N_{eb}, then the *seed_index* is calculated as:

$$seed\_index = N_{eb} / N_b \quad (1)$$

Image objects with *seed_index* equal to zero are considered to be edge free, and they are, thereby, selected as ocean seeds. In Figure 4d, the object 'obj 1' satisfies the *seed_index* condition but object 'obj 2' does not. The result of ocean seeds (blue objects) selection for the subimage is shown in Figure 4e, which demonstrates that no objects from the aquacultural area have been selected as ocean seeds.

Ocean Candidate Objects Selection

Candidate objects should satisfy two conditions: (1) they should be the direct neighbor of seed objects, and (2) should be 'water' objects. The first condition can be judged by spatial relationship and the second can be judged by band intensity. The second condition filters out non-water objects as candidates and could save the computation cost in the following merging step, by predefining a fixed

threshold value in the ocean seed selection step. In Figure 4f, candidate objects selected in the first round of iteration are shown in green.

Figure 5. Illustration of (**a**) border pixels of an object and (**b**) common boundary pixels of two image objects.

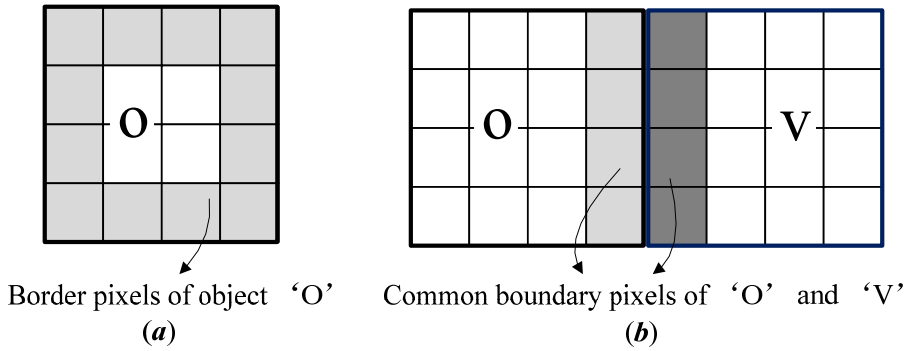

Ocean Object Growing

The OBRGIE method replies on the edge information to grow ocean objects, it is assumed that edges can hardly exist along the common border of a true ocean object and an ocean seed object, but they appear along the common border of a true ocean object and an aquaculture object, or other land object. This characteristic of edges is represented by a new feature, *OMI* (*object merging index*), which is used for the judgment of proper candidates for ocean growing.

The *OMI* value for a candidate is calculated in the following steps: (*i*) segment the selected candidate and the neighboring seed objects into pixels by chessboard segmentation and create an object level below (pixel level); (*ii*) identify the common boundary pixels (see Figure 5b) of the candidate object and the neighboring ocean seed, count the number as N_{cb}; and (*iii*) identify edge pixels among the common border pixels, and count the number of edge pixels as N_{ecb}, then the *OMI* value for the candidate is calculated as:

$$OMI = N_{ecb} / N_{cb} \quad (2)$$

The *OMI* value represents the percentage of the edge pixels among the common boundary pixels of the seed and the candidate, and it is in the range from 0 to 1. It is assumed that the *OMI* values for ocean candidates are close to 0, whereas non-ocean candidates have *OMI* value close to 1 (discussed in Section 5.1). The candidates belonging to the ocean can be separated from the non-ocean candidates by applying a threshold *OMI* value, then the ocean seeds grow to candidates which satisfy the *OMI* threshold condition, and the increased region is selected as the new seeds for the next growing iteration. The iteration stops when no candidates are available for growing. The ocean object growing processing for the subimage is illustrated in Figure 4g.

3.1.4. Post Processing

Post processing includes four tasks: lake removal, ship removal, boundary refinement, and vectorization. When processing large images with wide geospatial coverage, some large lakes may be extracted as ocean. These water regions will be removed if they are enclosed by the land region. In the

same way, ships in the ocean are removed if they are enclosed by ocean objects. The *area* attribute of the object is defined to avoid large island being removed as ships. Boundary refinement is based on mathematical morphological operations [25], and morphological opening and closing operation are used to generalize the jagged boundaries of image objects, making the coastline morphologically smoother (Figure 4h). Finally, the rater representation of land ocean boundary is converted into a vector format, and the Douglas-Peucker [26] algorithm is employed to simplify the boundary line (Figure 4i).

3.2. Accuracy Assessment Method

In accuracy assessment, the baseline approach, also known as the transact method, is used, which was first proposed by Dolan *et al.* [27] for determining the degree of shoreline resession. Thiele, *et al.* [28] developed an ArcGIS™ extension, the Digital Shoreline Analysis System (DSAS), to automate the process of calcating shoreline changes. In this study, we employ the DSAS tool to calculate the degree of matching between the true coastline and the test coastline, and detailed information about DSAS can be found on the following website, http://woodshole.er.usgs.gov/project-pages/dsas/.

Figure 6. Illustration of the baseline approach for accuracy assessment. x_i represents the length of a transact segment between the true coastline and the test line.

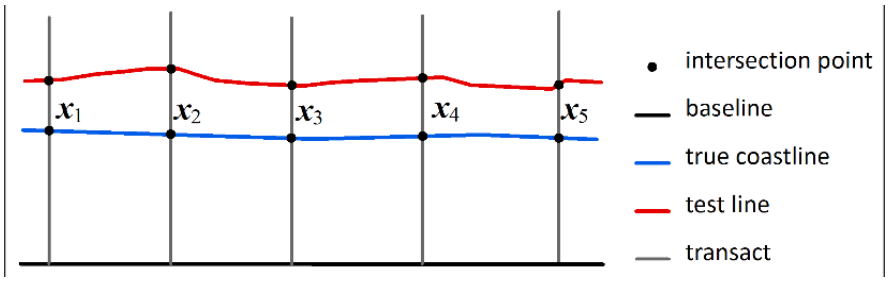

As illustrated in Figure 6, a baseline is, at first, determined. Transacts are then generated perpendicular to the baseline, and these transacts should intersect with the true coastline and the testline. For the *i*th transact, the distance between the two intersection points is denoted as x_i, which is calculated as Net Shoreline Movement (NSM) in DSAS. From these NSMs, we compute two statistical measures to represent the degree of matching between a test line and the true coastline - the mean and RMSE (root mean square error). These measures are calculated as:

$$mean = \frac{1}{n}\sum_{i=1}^{n}|X_i| \tag{3}$$

$$RMSE = \sqrt{\frac{1}{n}\sum_{i=1}^{n}(X_i - \bar{X})^2} \tag{4}$$

where n is the total number of transacts.

Two more measures are used to represent the closeness between a test line and the true coastline: (1) P_{GSD}—the percentage of the testline within 1 pixel distance (ground sample distance, GSD) of the true coastline; (2) $D_{90\%}$—the distance within which 90% of the testline are included.

3.3. Multiscale Analysis for OBRGIE

The segmentation step produces the image object primitives for ocean growing, and the segmentation result depends on the value of the scale parameter. In order to understand how the accuracy of extracted coastline changes when the scale parameter varies, we design an experiment to study the influence of the scale parameter on the accuracy of the coastline extracted with the OBRGIE method. In the Bohai case, the scale parameter value is increased from 10 to 60 with a step value of 10 for the Landsat TM image; in the Zhujiangkou case, the scale parameter value is increased from 10 to 30 with a step value of 5. The accuracies of the coastlines extracted by the OBRGIE method, with these scale values, are then computed.

3.4. Region Growing with Spectral Attributes for Coastline Extraction

White and El Asmar [29] used region growing algorithms for coastline extraction, but they used spectral attributes to grow the ocean region. In the OBRGIE method, we use the *OMI* feature for ocean growing. To demonstrate the effectiveness of the *OMI* feature, the region growing with spectral attributes (RGSA) method, by White and El Asmar [29], is used to produce coastlines in comparison with those generated by OBRGIE in both study cases.

In this study, the RGSA method shares almost the same work flow with the OBRGIE method, thus, we only change the *OMI* feature to the *SA* (spectral attribute) in the ocean object growing step. The *SA* value of an object primitive is computed as the mean object value of an NIR band. We select TM band-5 for the Bohai case and SPOT band-3 for the Zhujiangkou case, respectively, as these NIR bands are considered to reveal greater variation resulting from the difference between the reflectance of the land and the water [30]. The accuracy measures of the extracted coastlines are then calculated and compared.

4. Results and Analysis

4.1. Result of Coastline Extraction by OBRGIE

Figure 7 illustrates the processing sequences of OBRGIE applied to the TM image in the Bohai case. The ocean seed selection result in Figure 7a shows that most of the selected seed objects are located in the ocean, with only three located in large lakes on the land side. After the step of region growing with *OMI* features, almost the exact profile of the ocean region has been delineated (Figure 7b). Small features are removed and land-ocean boundaries are smoothed after post processing (Figure 7c). The OBRGIE method provides a visually representative coastline (Figure 7d) in a relatively long coastline (272 km). Three subareas in Figure 7d–f show that despite small errors along some coast segments, this method successfully captured the land-ocean boundary, even in complex areas with landward water features.

Figure 7. Automated coastline extraction from TM imagery in the Bohai case: (**a**) ocean seed selection result (blue) dropped on the TM band 5; (**b**) ocean (blue) identified by region growing; (**c**) land-ocean separation after post-processing; (**d**) extracted coastline (yellow) dropped on TM band 5; (**e**–**g**) magnified coastline segments with landward water features.

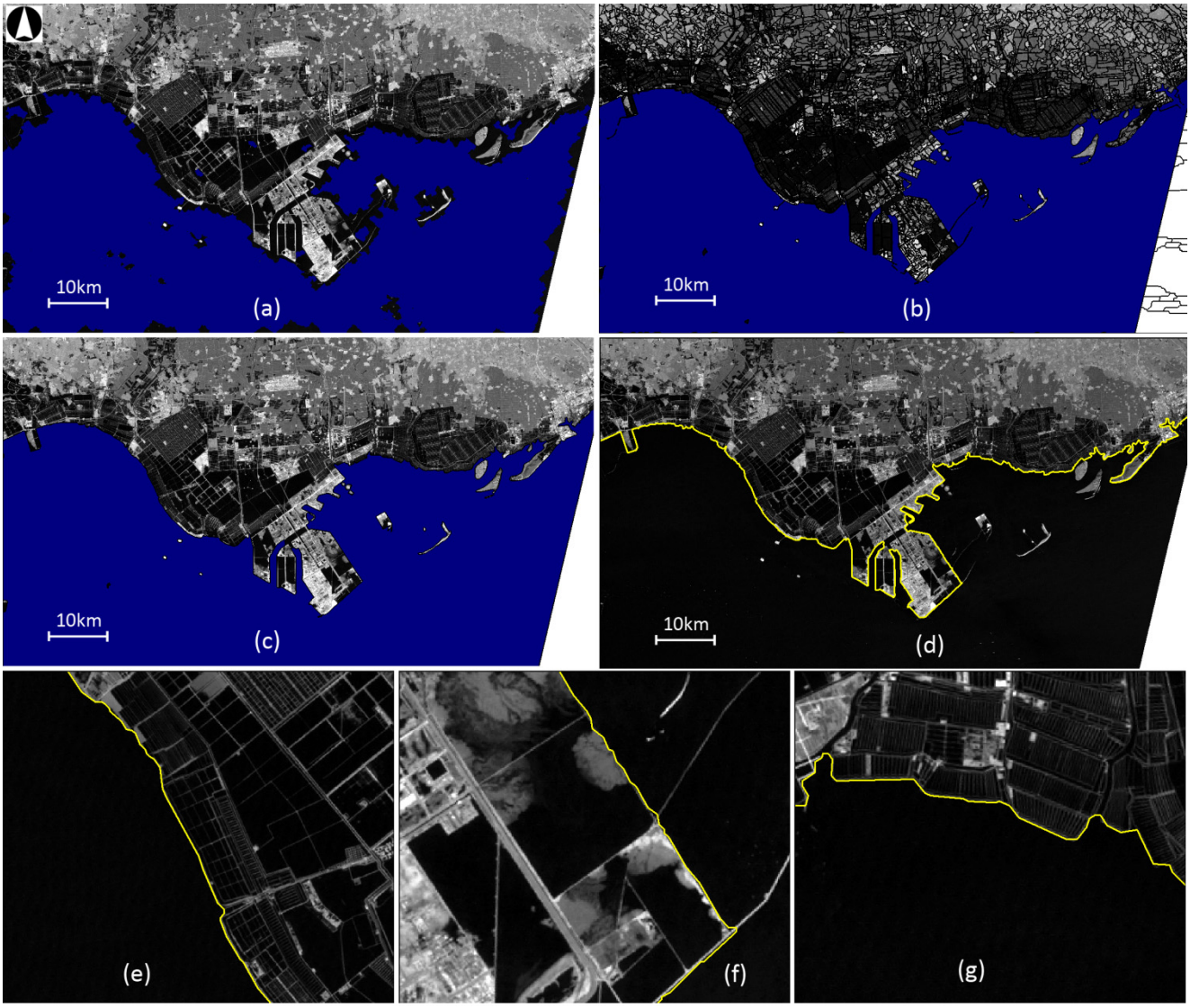

The coastline detection result of the SPOT-5 image by the OBRGIE method is shown in Figure 8. Result from Figure 8a–c shows that this method captures the ocean region with success, without confusing with water feature on the land side. The delineated coastline appears concave to the land side (Figure 8d), as there are many narrow channels along the coast and the spatial resolution (10 m) of the image is relatively high. Figure 8e,g shows two complex subareas with landward water features and the coastline extracted is visually acceptable.

Figure 8. Automated coastline extraction from SPOT-5 imagery (10m) in the Zhujiangkou case: (**a**) ocean seed selection result (blue) dropped on the SPOT-5 NIR band; (**b**) ocean (blue) identified by region growing; (**c**) land ocean separation after post-processing; (**d**) extracted coastline (yellow) dropped on TM band 5; (**e–f**) and (**g–h**) illustrate the magnified coastline segments with landward water features.

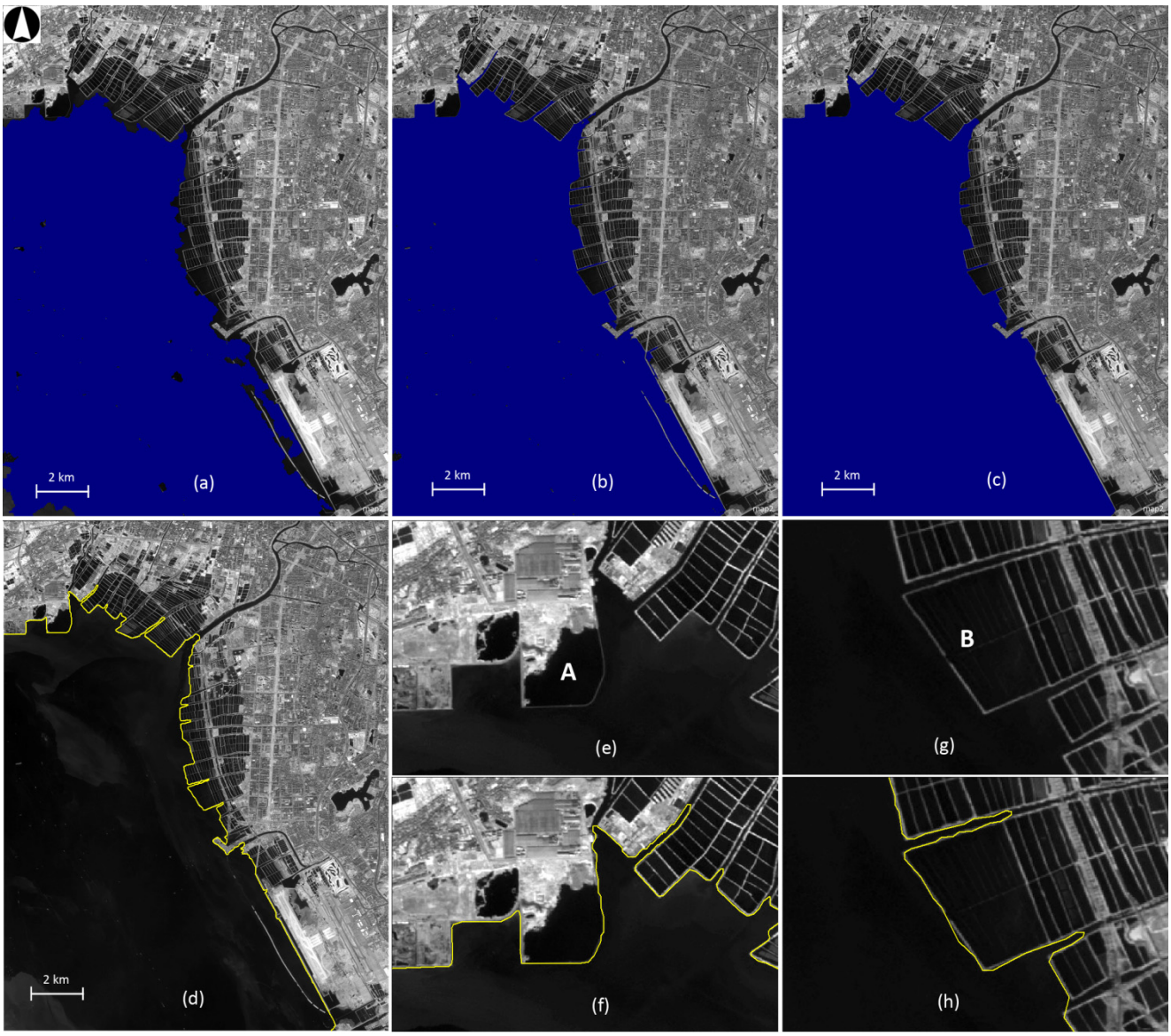

4.2. Multiscale Analysis Result with OBRGIE

Multiscale analysis with the OBRGIE method generates several coastlines on different segmentation scales, and the accuracy measures of these coastlines are shown in Figure 9. In both study cases, the accuracy lines remain stable, while the scale value varies, although the mean and RMSE value rise slightly when the scale value increases from 30.

The result indicates that the OBRGIE method is not sensitive to the segmentation scale, and a range of scale values can generate coastline with good accuracy. Therefore, there is no need to find the "optimal" segmentation scale and a fixed scale value is applicable to different coastal areas. It should be noted that extremely large or very small values of scale parameter are not applicable to the

OBRGIE method. We suggest users set the scale parameter to 30 for TM images and 15 for SPOT-5 multispectral images when applying the OBRGIE method for land-sea separation in practice.

Figure 9. Accuracy measures (mean and RMSE) of coastlines extracted by the OBRGIE method under different segmentation scale values for (**a**) Bohai case and (**b**) Zhujiangkou case.

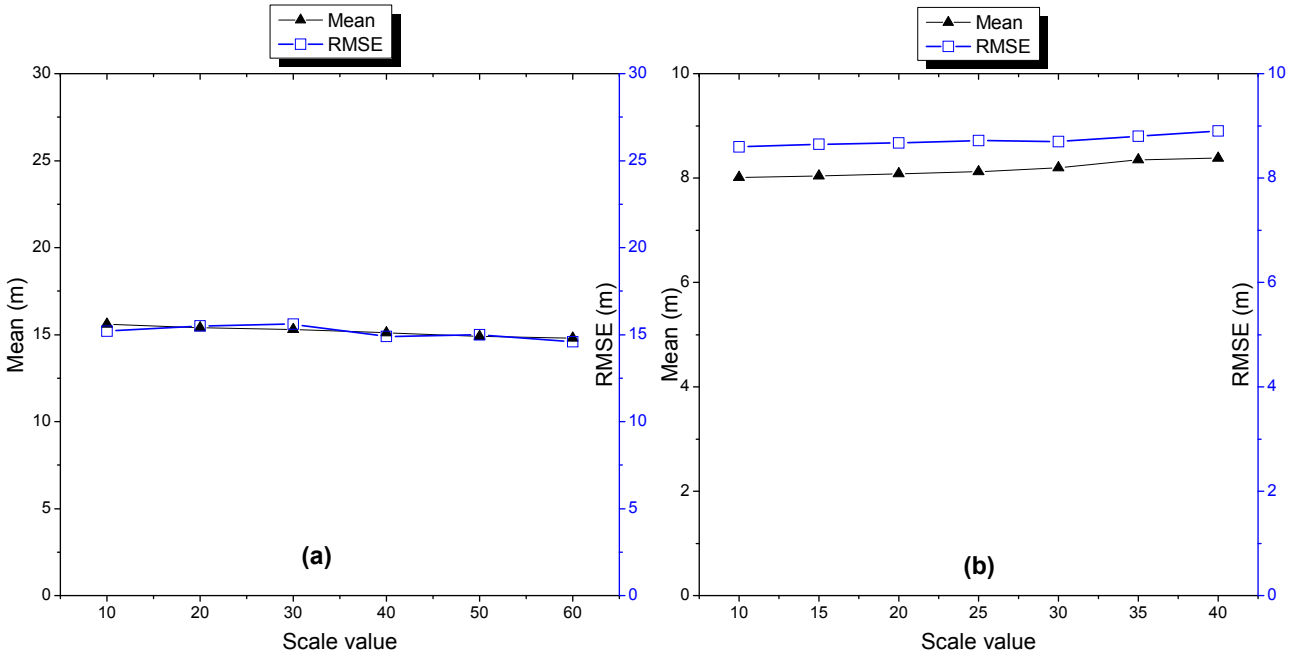

4.3. Quantitative Comparison between OBRGIE and RGSA

The *OMI* feature is used in the OBRGIE method for land-ocean separation, while the spectral attribute is used in the RGSA method. Table 2 shows the quantitative accuracy measures for the coastlines extracted by the OBRGIE and RGSA methods.

The OBRGIE method generates coastlines with good accuracy in both study cases. In the Bohai case, the mean and RMSE value obtained is about 16 m, half the value of the pixel size (30 m) of TM image, and 84.5% of the coastline segments lie within 1 pixel distance of the true coastline. In the Zhujiangkou case, the RMSE is 8.6 m and mean is 8.0 m, and 74.2% of the extracted coastline lies within 1 pixel distance (10 m) of the true coastline.

The RGSA method provides less accurate coastlines (Table 2). The mean is 31.7 m and RMSE is 80.5 m in the Bohai case, and 77.2% of the extracted line is within 1 pixel distance (30 m) of the true coastline. In the Zhujiangkou case, 63.1% of the extracted line by RGSA is within 1 pixel distance (10 m) of the true coastline, which is 10% less than that obtained by the OBRGIE method. The relatively large values of mean (54.3 m) and the RMSE (136.1 m) obtained by RGSA are caused by outliers in coastline segments. Figure 10 shows the condition of outliers in two coastline segments for which the RGSA method failed to capture the position of the true coastline.

Result shows that the OBRGIE method generates coastlines with better accuracy than the RGSA method, indicating that the *OMI* feature is more effective that spectral attributes for land-ocean separation in complex aquaculture coasts.

Table 2. Closeness of the extracted coastline to the true coastline indicated by RMSE, mean, $D_{90\%}$ (the distance within which 90% of the testline are included.), and P_{GSD} (the percentage of the testline within 1 pixel distance of the true coastline.). OBRGIE is the proposed method, using the new OMI feature for region grow, and RGSA is the method using spectral feature. The pixel size of image is 30 m in the Bohai case and 10 m in the Zhujiangkou case.

Cases	Methods	Accuracy Measures			
		RMSE(m)	Mean(m)	90% within (m) $D_{90\%}$	Within 1 Pixel (%) P_{GSD}
Bohai	OBRGIE	16.4	16.0	37.4	84.5
	RGSA	80.5	31.7	48.2	77.2
Zhujiangkou	OBRGIE	8.6	8.0	15.1	74.2
	RGSA	136.1	54.3	213.5	63.1

Figure 10. Illustration of outliers of coastline segments by RGSA method in (**a**) coastal area with a large lake and narrow dam, and (**b**) aquaculture region with channels and ponds.

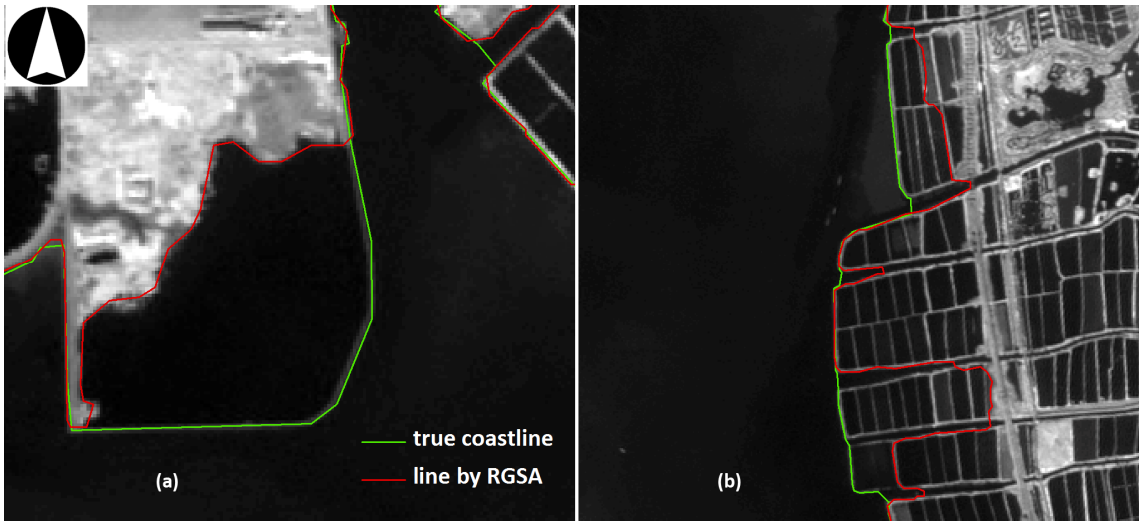

5. Discussion

5.1 OMI vs. *Spectral Attribute in Ocean Growing*

To better understand why the *OMI* feature is more effective, the histograms of *OMI* and *SA* (NIR band mean) features of candidate objects in the object growing step are studied. Figure 11 shows the frequency distribution histogram of *OMI* and *SA*. The histogram graph of the *OMI* feature clearly shows two peaks, indicating that the candidates objects can be easily separated into two groups. In contrast, the histogram for *SA* values shows only one peak, thus, it is difficult to find a threshold value to divide the candidate objects. Although the NIR band was considered to be effective in separating the land and the sea, as reported in previous research [2,30,31], results of this study show that the spectral feature is not enough to separate the sea and aquaculture ponds in complex aquaculture coasts. Instead, the *OMI* feature shows good adaptability in aquaculture coasts under object based context, so the OBRGIE method can generate coastlines with good accuracy.

Figure 11. Histograms for *OMI* and *SA* features of candidate objects in object growing processing. *SA* is the object mean of NIR band.

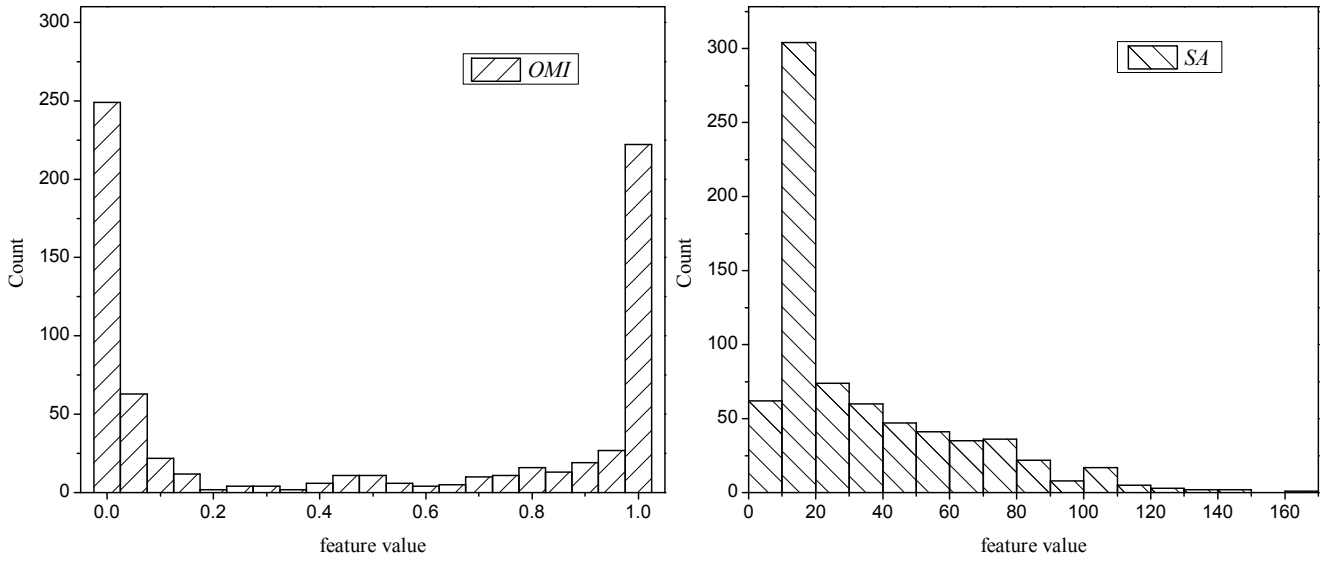

5.2. Limitations and Uncertainties

The first limitation for the proposed procedure lies in the unsatisfying performance in detecting shoreline changes for coastal segments with low rates of variation. As addressed by Gens [2], the accuracy of shoreline detection depends on the spatial resolution of the source image. The pixel accuracy of coastlines derived from low-resolution satellite imagery may not be good enough to capture small changes along the coast. Sub-pixel mapping approaches [13,14,30] may provide good alternatives under these situations, but these methods were only tested on short coastline sectors. In fact, coastlines with pixel level accuracy can be used as *a priori* knowledge and be useful for sub-pixel coastline mapping. For example, pixel level coastline extraction is a critical step for sub-pixel coastline mapping in the approach proposed by Pardo-Pascual *et al.* [30]. Therefore, combining sub-pixel mapping algorithms with the OBRGIE procedures may provide good potential for mapping coastlines with sub-pixel accuracy in relatively long coastal sectors.

Secondly, the method may fail to capture the real coastline position in coastal areas having large tidal ranges. In the case of tidal flats, especially during the ebb tide, large areas may be swamped close to the shoreline, as pointed out in [31]. In fact, the delineated line by the method is waterline, and the position of low tide waterline should deviate from the position of High Water Line (HWL) on tidal fat areas; the HWL is usually considered as a better indicator for shoreline position [2]. Therefore, the tidal effect should be taken into account when applying the method to silty coasts with large areas of tidal flats, and high tide time imagery is necessary to ensure that the line delineated is High Water Line.

6. Conclusion

Automated coastline mapping for aquaculture coasts is a difficult task due to the spatial and spectral complexities of these coastal segments. This study aims to make a contribution by proposing a new automated method (*object-based region growing integrating edge detection, OBRGIE*) for mapping

aquaculture coastline from multispectral imagery. The method combines image segmentation, region growing, and edge detection in the processing chain, and a new feature—*object merging index* (*OMI*) is proposed to utilize edge information in the key step of region growing. Test results show that the method derives coastlines with pixel accuracy, either from Landsat TM imagery, or from SPOT-5 imagery, in relatively long coastal sectors (272.7 km and 35.5 km). The proposed *OMI* feature has been demonstrated to be more effective than spectral attributes for separating coastal sea-water bodies and aquacultural water bodies. Furthermore, the method is robust to segmentation scale parameter, which means there is no need for the tiresome parameter tuning when applying the method.

The method could derive coastlines with pixel level accuracy in an automated way from relatively fine-to-moderate spatial resolution imagery (such as SPOT, Landsat TM/ETM+), and it may provide an inexpensive means of mapping coastlines with large spatial coverage. As the pixel level accuracy from low resolution imagery may not be good enough to detect small changes along coasts, future work will be focused on combing super-resolution techniques with the OBRGIE procedures, and it is expected to provide sub-pixel accuracy for relatively long coast sectors.

Acknowledgements

This work was supported in part by the National Natural Science Foundation of China (No. 40971224), and in part by the "863" Project of China (No. 2012AA121201, 2011AA120101). The authors would like to thank the editor and all the reviewers for their helpful suggestions and comments on this paper.

Conflict of Interest

The authors declare no conflict of interest.

References:

1. Boak, E.H.; Turner, I.L. Shoreline definition and detection: A review. *J. Coastal Res.* **2005**, *21*, 688–703.
2. Gens, R. Remote sensing of coastlines: Detection, extraction and monitoring. *Int. J. Remote Sens.* **2010**, *31*, 1819–1836.
3. Wang, C.Y.; Zhang, J.; Ma, Y. Coastline interpretation from multispectral remote sensing images using an association rule algorithm. *Int. J. Remote Sens.* **2010**, *31*, 6409–6423.
4. Gao, Y. Research on Spatial and Temporal Changes of China mainland Coastline in the Past 30 Years (in Chinese). Ph.D. Dissertation; Graduate University of Chinese Academy of Sciences, Beijing, China, 2011.
5. Mason, D.C.; Davenport, I.J. Accurate and efficient determination of the shoreline in ERS-1 SAR images. *IEEE Trans. Geosci. Remote Sens.* **1996**, *34*, 1243–1253.
6. Liu, H.X.; Jezek, K.C. A complete high-resolution coastline of antarctica extracted from orthorectified Radarsat SAR imagery. *Photogramm. Eng. Rem. Sens.* **2004**, *70*, 605–616.
7. Sohn, H.G.; Jezek, K.C. Mapping ice sheet margins from ERS-1 SAR and SPOT imagery. *Int. J. Remote Sens.* **1999**, *20*, 3201–3216.

8. Kuleli, T.; Guneroglu, A.; Karsli, F.; Dihkan, M. Automatic detection of shoreline change on coastal Ramsar wetlands of Turkey. *Ocean Eng.* **2011**, *38*, 1141–1149.
9. Maiti, S.; Bhattacharya, A.K. Shoreline change analysis and its application to prediction: A remote sensing and statistics based approach. *Mar. Geol.* **2009**, *257*, 11–23.
10. Yamano, H.; Shimazaki, H.; Matsunaga, T.; Ishoda, A.; McClennen, C.; Yokoki, H.; Fujita, K.; Osawa, Y.; Kayanne, H. Evaluation of various satellite sensors for waterline extraction in a coral reef environment: Majuro Atoll, Marshall Islands. *Geomorphology* **2006**, *82*, 398–411.
11. Kingston, K.S.; Ruessink, B.G.; van Enckevort, I.M.J.; Davidson, M.A. Artificial neural network correction of remotely sensed sandbar location. *Mar. Geol.* **2000**, *169*, 137–160.
12. Guariglia, A.; Buonamassa, A.; Losurdo, A.; Saladino, R.; Trivigno, M.L.; Zaccagnino, A.; Colangelo, A. A multisource approach for coastline mapping and identification of shoreline changes. *Ann. Geophys.* **2006**, *49*, 295–304.
13. Foody, G.M.; Muslim, A.M.; Atkinson, P.M. Super-resolution mapping of the waterline from remotely sensed data. *Int. J. Remote Sens.* **2005**, *26*, 5381–5392.
14. Muslim, A.M.; Foody, G.M.; Atkinson, P.M. Localized soft classification for super-resolution mapping of the shoreline. *Int. J. Remote Sens.* **2006**, *27*, 2271–2285.
15. Lee, D.S.; Shan, J. Combining lidar elevation data and IKONOS multispectral imagery for coastal classification mapping. *Mar. Geod.* **2003**, *26*, 117–127.
16. Deronde, B.; Houthuys, R.; Debruyn, W.; Fransaer, D.; Van Lancker, V.; Henriet, J.P. Use of airborne hyperspectral data and laserscan data to study beach morphodynamics along the Belgian coast. *J. Coastal Res.* **2006**, *22*, 1108–1117.
17. Benz, U.C.; Hofmann, P.; Willhauck, G.; Lingenfelder, I.; Heynen, M. Multi-resolution, object-oriented fuzzy analysis of remote sensing data for GIS-ready information. *ISPRS J Photogramm. Remote Sens.* **2004**, *58*, 239–258.
18. Trimble. *eCognition Developer 8.7: Reference Book*; Trimble: Munich, Germany, 2011.
19. Blaschke, T. Object based image analysis for remote sensing. *ISPRS J Photogramm. Remote Sens.* **2010**, *65*, 2–16.
20. Polychronaki, A.; Gitas, I.Z. Burned area mapping in greece using SPOT-4 HRVIR images and object-based image analysis. *Remote Sens.* **2012**, *4*, 424–438.
21. Salehi, B.; Zhang, Y.; Zhong, M.; Dey, V. Object-Based Classification of Urban Areas Using VHR Imagery and Height Points Ancillary Data. *Remote Sens.* **2012**, *4*, 2256–2276.
22. Tarantino, E.; Figorito, B. Mapping Rural Areas with Widespread Plastic Covered Vineyards Using True Color Aerial Data. *Remote Sens.* **2012**, *4*, 1913–1928.
23. Vo, Q.; Oppelt, N.; Leinenkugel, P.; Kuenzer, C. Remote sensing in mapping mangrove ecosystems—An object-based approach. *Remote Sens.* **2013**, *5*, 183–201.
24. Canny, J. A computational approach to edge-detection. *IEEE Trans. Pattern Anal. Mach. Intell.* **1986**, *8*, 679–698.
25. Serra, J. *Image Analysis and Mathematical Morphology*; Academic Press: London, UK, 1982.
26. Douglas, D.H.; Peucker, T.K. Algorithms for the reduction of the number of points required to represent a digitized line or its caricature. *Cartographica: Int. J. Geogr. Inf. Geovisual.* **1973**, *10*, 112–122.

27. Dolan, R.; Hayden, B.; Heywood, J. New photogrammetric method for determining shoreline erosion. *Coast Eng.* **1978**, *2*, 21–39.
28. Thieler, E.; Himmelstoss, E.A.; Zichichi, J.L.; Ergul, A. *The Digital Shoreline Analysis System(DSAS) Version 4. 0—An ArcGIS Extension for Calculating Shoreline Change*; USGS: Woods Hole, MA, USA, 2009.
29. White, K.; El Asmar, H.M. Monitoring changing position of coastlines using Thematic Mapper imagery, an example from the Nile Delta. *Geomorphology* **1999**, *29*, 93–105.
30. Pardo-Pascual, J.E.; Almonacid-Caballer, J.; Ruiz, L.A.; Palomar-Vázquez, J. Automatic extraction of shorelines from Landsat TM and ETM+ multi-temporal images with subpixel precision. *Remote Sens. Environ.* **2012**, *123*, 1–11.
31. Ryu, J.H.; Won, J.S.; Min, K.D. Waterline extraction from Landsat TM data in a tidal flat—A case study in Gomso Bay, Korea. *Remote. Sens. Environ.* **2002**, *83*, 442–456.